Magnetic dipole transitions in titaniumlike ions

H. Watanabe,[1] D. Crosby,[2] F. J. Currell,[1,3] T. Fukami,[4] D. Kato,[1] S. Ohtani,[1,4] J. D. Silver,[2] and C. Yamada,[1,4]
[1]*Cold Trapped Ions Project, ICORP, Japan Science and Technology Corporation (JST), Tokyo 182-0024, Japan*
[2]*Clarendon Laboratory, University of Oxford, Oxford, OX1 3PU, United Kingdom*
[3]*The Queen's University of Belfast, Belfast, BT7 1NN, United Kingdom*
[4]*University of Electro-communications, Tokyo 182-8585, Japan*
(Received 12 May 2000; revised manuscript received 22 November 2000; published 21 March 2001)

Visible and near-UV emission lines of titaniumlike highly charged ions Sb, I, Xe, Ba, Cs, Sm, Eu, Hf, Ta, W, Re, and Pt were observed using an electron beam ion trap. The wavelengths of the magnetic dipole transitions between ground-state fine-structure levels, $(3d^4)^5D_J$, were measured for these elements. These were compared with our own theoretical values, which were obtained with an extended set of configurations, and yielded differences of less than 0.6% for the elements below $Z=60$, and about 0.1% for those over $Z=60$.

DOI: 10.1103/PhysRevA.63.042513 PACS number(s): 32.30.Jc, 32.10.Fn, 31.15.Ar, 52.70.−m

I. INTRODUCTION

Accurate measurements of transition energies between the ground-state configurations of highly charged ions are important for an understanding of the atomic structure in many-electron systems. In addition, the systematic observation and identification of intense lines in the visible region are also important for plasma diagnostics to measure the ion temperature, density distribution, and local magnetic field strength [1–3]. The transition lines within the $3s^23p^k$ ground state for plasma impurity ions such as Ti, Fe, Ge, and Mo have been systematically observed [3–6]. However, in plasmas with temperatures over 5 keV, which are being achieved in the new generation of plasma devices, these lines cannot be used, since the ions will be ionized to higher charge states. Instead, other transitions become useful in higher charge state: high-Z ions with higher ionization potentials.

Feldman, Indelicato, and Sugar [7] conducted a search for new forbidden transition lines of highly charged ions with ionization energies of 5–10 keV, which could be suitable for plasma diagnostics at optical wavelengths. This search employed a multiconfiguration Dirac-Fock (MCDF) method to perform *ab initio* calculations of candidate transitions. They found a sequence of magnetic dipole transitions between the fine-structure levels of the $(3d^4)^5D_J$ $(J=2,3)$ ground terms in Ti-like ions that appeared in the visible and near-UV region over a wide range of atomic number.

The wavelengths of these transitions have been measured for Xe, Ba, Nd, Gd, Yb, W, Au, and Bi with the Lawrence Livermore National Laboratory (LLNL), the National Institute of Standards and Technology (NIST), and Oxford electron beam ion traps (EBIT's) [8–14]. The theoretical results obtained by Feldman, Indelicato, and Sugar [7] reproduced the experimental results fairly well, but the absolute values differ by about 5% from the measured ones. Thereafter there were some attempts to improve theoretical wavelengths. The differences in the results of Beck [15] were reduced to 1–2 % for Xe, Ba, Gd, and Nd. Recently Beck [16] reported the theoretical wavelengths for W and Bi, which were compared with the experimental values measured by Porto, Kink, and Gillaspy [10]. The differences were about 0.7% for W and 0.06% for Bi. These demonstrate that systematic measurements of atomic transitions are indispensable to refining calculations of the atomic structure of many body systems.

In this study we have measured the wavelengths of the $(3d^4)^5D_2$-$^5D_3$ transition in Ti-like Sb ($Z=51$), I ($Z=53$), Xe ($Z=54$), Cs ($Z=55$), Ba ($Z=56$), Sm ($Z=62$), Eu ($Z=63$), Hf ($Z=72$), Ta ($Z=73$), W ($Z=74$), Re ($Z=75$), and Pt ($Z=78$) ions. According to Feldman, Indelicato, and Sugar [7] the energy of $J=4$ level becomes almost the same as that of $J=2$ at around $Z=63$. Both the $(3d^4)^5D_2$-$^5D_3$ and $(3d^4)^5D_4$-$^5D_3$ transitions appear in the same wavelength region. We have measured the wavelengths of these two transitions simultaneously for Ti-like Sm ($Z=62$) and Eu ($Z=63$) ions. Since the $(3d^4)^5D_2$-$^5D_3$ and $(3d^4)^5D_4$-$^5D_3$ transitions have the same upper level, the intensity ratio should be connected with the lifetime ratio and also with the branching ratio. We obtained the branching ratio of the $(3d^4)^5D_2$-$^5D_3$ transition in Sm ions by calibrating the intensities relatively. Electron beam energies higher than 2 keV were needed to produce sufficient trapped Ti-like ions for the elements measured in this study. The identification of these lines is considered to be particularly important for diagnostics of high-temperature plasmas. Recently, we also performed *ab initio* calculations with the MCDF method for various elements besides those calculated by Beck [15,16]. The calculated wavelengths are compared with the data obtained in the experiments.

II. EXPERIMENT

The experimental setup is shown in Fig. 1. The Tokyo-EBIT [17,18], constructed at the University of Electro-Communications, was used to produce and trap highly charged ions. An electron beam emitted from an electron gun was accelerated toward a trap region, and compressed by an axial magnetic field produced by superconducting magnets. Ions produced in the trap were subjected to further electron-impact ionization, resulting in the production of highly charged ions. The maximum electron beam energy and current of the Tokyo-EBIT were designed to be 300 keV and 300 mA, respectively. However, in this study a much lower-

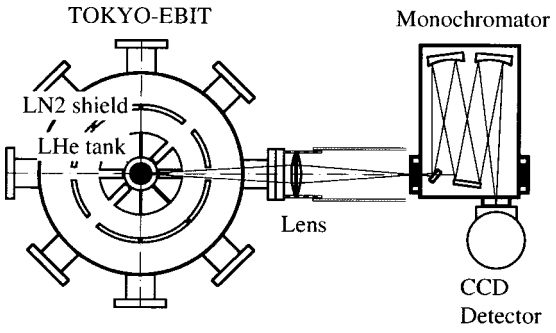

FIG. 1. Experimental setup for visible spectroscopy. LN2 and LHe denote liquid nitrogen and liquid helium, respectively. The cross-sectional view of the EBIT at the center of the drift tube is shown.

energy beam was used so that the generation of Ti-like ions was optimized. At such low beam energies it was difficult to transport a stable electron beam without serious loss of electrons to the inner surfaces of the device. For a given beam energy, the EBIT was tuned to give the maximum beam current obtainable.

Source elements were introduced into the trap by various methods. Sb was injected into the trap as an organometallic compound, $Sb(CH_3)_3$, via a gas injection port. I_2 and Xe were also introduced through this port. Cs was injected from the top of the EBIT as singly charged ions from a Cs ion source (Heat Wave aluminosilicate ion source). Ba was evaporated from the cathode of the EBIT electron gun and thereafter ionized in the trap. A metal vapor vacuum arc (MEVVA) ion source, which was fitted above the EBIT, was used to inject low-charged ions of metallic elements as Sm, Eu, Hf, Ta, W, Re, and Pt. The MEVVA was fired every 4 s. In the present study, to avoid the contamination of emission lines from other elements, a coolant gas such as neon was not introduced into the trap.

Ions were trapped radially by the electric potential produced by the electron beam. The trap region of the Tokyo-EBIT consists of a series of three cylindrical electrodes, called drift tubes. Axial trapping was achieved by applying a positive potential to the end drift tubes. For Sb, I, Xe, Cs, and Ba measurements the voltage of the lower drift tube (i.e., nearest to the electron gun) was 150 V and that of the upper one 50 V with respect to the central drift tube. The voltage of the central drift tube was raised instantaneously every 20 s from 0 to 100 V to dump unwanted ions, which tend to accumulate in the trap. On the other hand, for the other measurements the voltage of the lower drift tube was 500 V and that of the upper one, 400 V. In this case, the voltage of the upper drift tube was lowered instantaneously every 4 s from 400 to 0 V to introduce source ions, synchronously with the MEVVA fire.

A biconvex fused silica lens with a focal length of 153.8 mm was used in this experiment. The diameter of the lens was 100 mm, although the effective diameter was about 40 mm after considering defocusing due to aberrations. Rays that passed outside the effective diameter could not hit the entrance slit of the monochromator. The monochromator was of a Czerny-Turner type (Jobin-Yvon HR320) with a focal length of 320 mm and an f number of 4.2. A grating of 600 grooves/mm, blazed at 750 nm was used in second order for the I, Xe, Cs, and Ba measurements, while a grating of 1200 grooves/mm, blazed at 400 nm was used in first order for the other measurements. The width of the entrance slit was 100 μm in all experiments. The lens and the monochromator were aligned on an optical axis defined by a laser beam. The lens was initially placed at 347 mm and the monochromator entrance slit at 612 mm from the electron beam axis of the EBIT, yielding an image demagnification factor of about 0.8. The position of the monochromator was optimized by maximizing the transmitted light intensity from the EBIT. A liquid-nitrogen-cooled charge-coupled device (CCD) detector (Princeton Instruments LN/CCD-1100-PB/VISAR) was placed in the focal plane of the monochromator. The CCD detector array consists of 1100×330 24-μm square pixels, which corresponded to a wavelength of about 0.055 nm in the configuration employed. The spectral coverage of a single image on the CCD was about 60 nm.

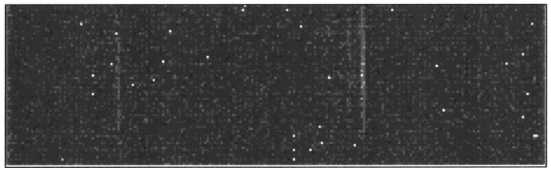

FIG. 2. CCD image of the iodine emission line. The exposure time was 30 min. The electron beam energy was 2.0 keV, and the current was 23 mA.

We obtained two-dimensional images at the focal plane of the monochromator. Figure 2 shows an example spectral image of I^{31+}, taken with a 30-min exposure. The many dots scattered around the image are most probably due to cosmic rays. To obtain spectral lines as a function of horizontal pixel position along the CCD, the intensity of each pixel was added vertically (columnwise). In doing so we eliminated any rows of pixels containing spikes. An accumulated spectrum was then obtained by adding several spectra together. The resulting spectra obtained are shown in Fig. 3. The experimental conditions are also shown in the figure.

III. RESULTS

The wavelength scale was calibrated using emission lines from standard lamps (He, Ne, Ar, Kr, and Hg) placed outside the EBIT, and shone through a fused silica window opposite to the monochromator port. Gaussian functions were fitted to obtain the centroid positions of the calibration lines, and thus determine the wavelengths corresponding to specific positions on the CCD. A third-order polynomial, deduced from the wavelength-position relation obtained in calibration, was used to convert the position scale to a wavelength scale.

A similar procedure used for the calibration lines was employed to determine the centroid positions of the observed lines in the spectra shown in Fig. 3. These results are tabulated in Table I for the $(3d^4)^5D_2$-$^5D_3$ transition, and in Table II for the $(3d^4)^5D_4$-$^5D_3$ transition. Also included are previous experimental and theoretical results, together with our theoretical results.

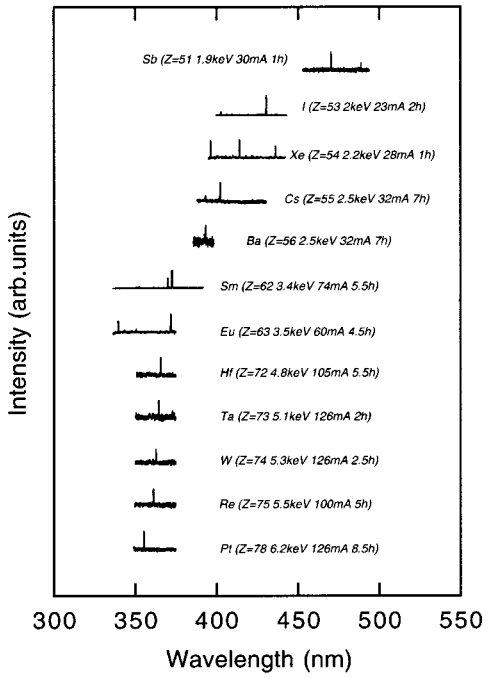

FIG. 3. The emission lines of Ti-like ions. The heights of spectra have been adjusted so that the height of the most intense line in each spectrum appears to be the same.

TABLE II. Wavelengths of the $(3d^4)^5D_4$-$^5D_3$ transition in Ti-like ions. The numbers in parentheses are experimental uncertainties. Wavelengths are values in air.

Z	Measured wavelengths (nm)	Calculated wavelengths (nm)
62 (Sm)	369.89(3)	371.20
63 (Eu)	339.48(4)	340.94

The measured errors were obtained by first taking the statistical uncertainty at each pixel, which arises from photon counting statistics, propagated into the wavelength value through the fitting procedure mentioned above. These errors were then added in quadrature to the uncertainty originating from the wavelength calibration due to the errors associated with measuring the centroid positions of the calibration lines on the CCD. The position of the external lamps was different from the trapped ions in the EBIT, which might be a cause of systematic errors. These were checked *in situ* by comparing the wavelengths we determined with those previously reported, which were measured several times in between the measurements reported here. Kaufman and Sugar [19] reported that the wavelengths of Kr^{22+} $^3P_1$-$^3P_2$ and Ar^{13+} $^2P_{1/2}$-$^2P_{3/2}$ were 384.09(3) and 441.24(2) nm, respectively. In this study the wavelength of Kr^{22+} $^3P_1$-$^2P_2$ was measured as 384.05(9), 384.05(4), and 384.08(4) nm, and that of Ar^{13+} $^2P_{1/2}$-$^2P_{3/2}$ was 441.26(8) nm. The values in the parentheses represent the standard errors. These results agreed

TABLE I. Wavelengths of the $(3d^4)^5D_2$-$^5D_3$ transition in Ti-like ions. The numbers in parentheses are experimental uncertainties. Wavelengths are values in air.

	This work (nm)		Prior work (nm)	
Z	Measured	Calculated	Measured	Calculated
51 (Sb)	470.24(3)	472.77		
53 (I)	430.33(8)	430.58		410.95[a]
54 (Xe)	413.88(7)	415.53	413.94(20)[b], 413.87[c]	395.25[a], 407.82[d]
55 (Cs)	402.14(11)	402.73		
56 (Ba)	393.08(12)	393.54	393.24(20)[b], 393.2[c], 393.239(8)[e]	386.53[d]
60 (Nd)		375.28	375.3(2)[f]	355.68[a], 367.83[d]
62 (Sm)	372.52(3)	372.28		
63 (Eu)	371.75(3)	371.64		
64 (Gd)		371.10	371.3(2)[f]	367.43[d]
70 (Yb)		367.57	367.64(15)[g]	356.45[a]
72 (Hf)	365.54(4)	365.33		
73 (Ta)	364.18(5)	363.97		
74 (W)	362.67(5)	362.47	362.6(2)[g], 362.713(10)[h]	354.61[a], 360.50[i]
75 (Re)	361.06(5)	360.81		
78 (Pt)	355.44(4)	355.11		
79 (Au)		353.00	353.2(2)[j]	
83 (Bi)		343.77	344.29(15)[g]	344.06[i]

[a]Feldman *et al.* [7].
[b]Morgan *et al.* [8].
[c]Crespo López-Urrutia *et al.* [12].
[d]Beck [15].
[e]Bieber *et al.* [11].
[f]Serpa *et al.* [9].
[g]Porto *et al.* [10].
[h]Utter *et al.* [13].
[i]Beck [16].
[j]Träbert *et al.* [14].

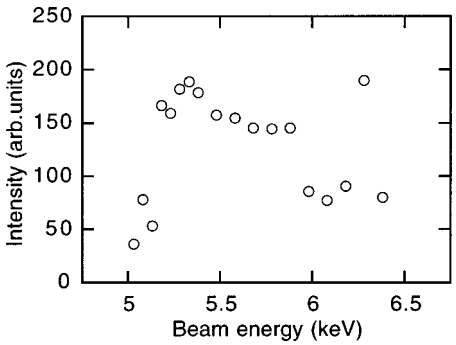

FIG. 4. The intensity variation of the line identified as the $(3d^4)^5D_2$-$^5D_3$ transition in Ti-like Re ions as a function of the beam energy. The energy value is corrected for the estimated potential drop (240 eV) of the electron beam.

within the quoted uncertainties, suggesting that our calibration procedure was reasonable.

We confirmed that the lines disappeared when the ion injection was stopped, and also checked that the appearance potentials of the measured lines were just above the ionization energies for the production of the Ti-like ions. In Fig. 4, as an example, the intensity of the observed $(3d^4)^5D_2$-$^5D_3$ $M1$ transition in Ti-like Re ions is shown as a function of electron beam energy. The actual value of the interaction energy should be corrected for the potential drop due to the space charge of the electron beam. With operating conditions of 100 mA and 5.5 keV, the correction value is calculated to be -240 eV, and is accounted for in the data of Fig. 4. As shown in this figure, the threshold for observation of the measured line was 2–300 eV above the ionization energy for the production of Ti-like Re ions, which is about 4.7 keV [20]. No other lines were observed in this wavelength region when we operated at a 4.7-keV electron beam energy. Similar results were obtained for the other elements. From these observations and with aid of the theoretical predictions, we confirmed the lines observed to be due to the $(3d^4)^5D_2$-$^5D_3$ transition of Ti-like ions. Figure 4 corresponds to the relative excitation function when we neglect the energy dependence of the polarizations.

We carried out MCDF calculations to obtain ground-state energies of the fine-structure levels of the Ti-like ions using the GRASP92 code [21], and subsequently obtained wavelengths of the $(3d^4)^5D_2$-$^5D_3$ and $(3d^4)^5D_4$-$^5D_3$ transitions. Details of the calculations will be presented in another paper [22]. The energy levels are plotted in Fig. 5, wherein the energy values of the $J=3$ levels are taken to be zero. In the low-Z region the orders of the energy levels are $J=4$, 3, 2, 1, and 0. Figure 5 demonstrates that the energies of the $J=2$ levels are almost constant with respect to those of the $J=3$ levels, resulting in a virtually Z-independent wavelength variation of the $(3d^4)^5D_2$-$^5D_3$ transitions. This contrasts with the other energy levels, which change rapidly with respect to Z when compared to each other. All the energy levels vary rapidly with respect to Z when considered in isolation. Over $Z=52$ the energy of the $J=4$ level is lower than that of the $J=3$ level, and at around $Z=62$ the energy

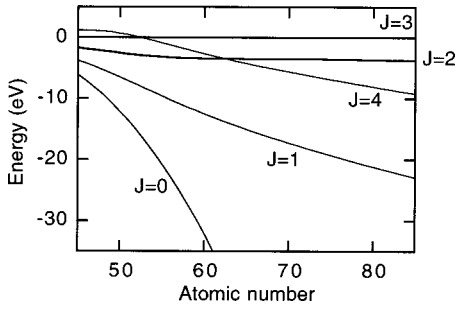

FIG. 5. The energy diagram of the ground-state fine-structure levels, calculated with the MCDF method. The energy value of the $J=3$ level is taken to be zero.

of the $J=4$ level has almost the same value as that of the $J=2$ level.

IV. DISCUSSION

A. Sb, I, Xe, Cs, and Ba

The lines observed at 470.24(3), 430.33(8), 413.88(7), 402.14(11), 393.08(12) nm are identified as the $(3d^4)^5D_2$-$^5D_3$ transitions in Ti-like Sb, I, Xe, Cs, and Ba ions, respectively. The line observed at 396.19(12) nm is a $(3d^5)\ ^4G_{7/2}$-$^4G_{9/2}$ transition in V-like Xe ions according to Morgan *et al.* [8], and that at 436.15(8) nm is a line of Kr-like Xe ions according to Refs. [12,23]. The line at 402.60(7) nm may be from lower charge state ions of I, since this line was still observed at a lower electron beam energy at which the line of Ti-like I ions disappeared.

The $(3d^4)^5D_2$-$^5D_3$ transitions in Ti-like Xe and Ba ions have already been observed by Morgan *et al.* [8]. Their results are consistent with ours, while our accuracy seems somewhat superior. Bieber *et al.* [11] reported the wavelength measurement in Ba^{34+}, together with measurements of Ba^{33+} and $Ar^{10+,13+,14+}$ in the visible region, with better accuracy than the others. However, their result is slightly outside the range of our uncertainty. Crespo López-Urrutia *et al.* [12] also reported the wavelengths for Ti-like Xe and Ba ions. Their results agree with ours within the range of our uncertainties. The theoretical results qualitatively reproduce the change of wavelength with respect to Z; however, the absolute values calculated by Feldman, Indelicato and Sugar [7] depart somewhat from the experimental ones. In our results the discrepancy has been reduced to less than 0.6%. This may be due mostly to the inclusion of higher excited-state configurations such as $3l^{-1}nl(4\leqslant n\leqslant 7; l'\leqslant 6)$ and $3d^{-2}nln'l'(4\leqslant n,n'\leqslant 6; l,l'\leqslant 5)$ which represent some of the electronic correlation effects missed in the calculations by Feldman, Indelicato, and Sugar [7].

B. Sm and Eu

As shown in Fig. 5, the $J=2$ and 4 levels have almost the same energy at around $Z=62$. Therefore both the $(3d^4)^5D_2$-$^5D_3$ and $(3d^4)^5D_4$-$^5D_3$ transition lines will be observed in the same wavelength region for Sm and Eu. The $(3d^4)^5D_2$-$^5D_3$ transitions were measured at 372.52(3) and 371.75(3) nm for Ti-like Sm and Eu ions, respectively, while

the calculated values were 372.28 and 371.64 nm. The differences between the experimental and theoretical values are less than 0.07% for both ions. The wavelengths of the $(3d^4)^5D_4$-$^5D_3$ transitions were 369.89(3) and 339.48(4) nm for Sm and Eu ions, respectively, while the calculated values were 371.20 and 340.94 nm. The differences of both the results are about 0.4%. Therefore, these are almost six times as large as those for the $(3d^4)^5D_2$-$^5D_3$ transition. In the present calculations, the orbital wave functions were optimized by making the sum of the $J=2$ and 3 level energies stationary with respect to a small change in their radial functions. It is suggested that the level energies for $^5D_2$ and $^5D_3$ are more accurate than the others. Thus the wavelengths of the $(3d^4)^5D_2$-$^5D_3$ transitions were accurate in comparison with those of the $(3d^4)^5D_4$-$^5D_3$ transitions.

As described before, the $J=4$ level, which is the highest energy level among the fine structures in the ground-state configuration at low Z, goes down and crosses the $J=3$ and 2 levels as Z increases. At high Z (over 62) the $(3d^4)^5D_4$-$^5D_3$ transition competes with the $(3d^4)^5D_2$-$^5D_3$ transition. Since it is of interest to observe a branching ratio to the $J=2$ level, we have estimated the branching ratio in the Ti-like Sm ($Z=62$) ion by observation of the relative intensity ratio between the $(3d^4)^5D_2$-$^5D_3$ and $(3d^4)^5D_4$-$^5D_3$ transitions. To do this, we first measured the sensitivity of the present optical detection system, including the monochromator to the polarization, by using the combination of a linear polarizer and several unpolarized emission lines ($J=1$-0 transitions) from Ne and Ar discharge lamps at around 370 nm. Second, we took account of the possible degree of the alignment produced on the initial state, $^5D_3$. The branching ratio of the $(3d^4)^5D_2$-$^5D_3$ transition was experimentally estimated to be about 67% if we assumed an unpolarized line emission. By using the maximum and the minimum values of the alignments, it was consequently estimated that the measured intensity ratio corresponds to a branching ratio ranging from 60% to 69%. The theoretical branching ratio for Sm^{40+} is 62.9%. Thus the theoretical value is slightly smaller than the experimental one. The present estimation of the experimental branching ratio is rather rough. Precise measurements of the polarizations are needed.

C. Hf, Ta, W, Re, and Pt

In this range of Z, the measurements for Yb, W, and Bi were performed at NIST [10], and those of W and Au at LLNL [13,14]. There are two different measurements for W; the result at NIST was 362.6(2) nm [10] and that at LLNL was 362.713(10) nm [13]. The wavelength in the present set of measurements was 362.67(5) nm. These results agree well with each other within the uncertainties. When we compare the values for W obtained in the present experiment and calculation, the agreement is rather good, and the difference is about 0.06%, while with Feldman, Indelicato, and Sugar [7] it is about 2%. For Hf, Ta, W, Re, and Pt ions measured in this study, the differences of the theoretical values from the experimental ones are almost constant and less than 0.1% (0.4 nm). However in the cases of Sb, I, Xe, Cs, and Ba ions, the differences were about four times larger than these ions. In Fig. 6 the differences are shown for all available data including those previously measured. Above $Z=60$ the differences are almost constant and less than 0.16%. Accuracy of the calculations for high Z elements are pretty good, while below $Z=60$ the differences suddenly become larger. In the region from $Z=40$ to 60 the coupling scheme changes from *LS* coupling to *JJ* coupling, where the state should be described with intermediate coupling. In the present calculations the basis functions with *JJ* coupling were used in solving MCDF equations. Over $Z=60$ the states are well described with *JJ* coupling. Thus the theoretical results over $Z=60$ were more accurate than those below $Z=60$.

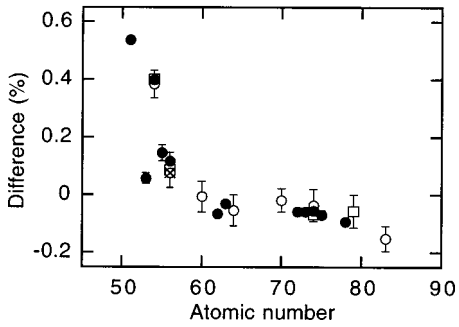

FIG. 6. The differences between our theoretical and the available experimental wavelengths. The values are defined as $(wl_{\text{th.}} - wl_{\text{ex.}})/wl_{\text{ex.}} \times 100$, where $wl_{\text{th.}}$ is the theoretical wavelength and $wl_{\text{ex.}}$ the experimental wavelength. ● are differences from the wavelength obtained using our measurements. ○ are those using the wavelengths measured by the NIST group [8–10], □ those of the LLNL group [12–14], and × those of the Oxford group [11].

V. CONCLUSION

In this study we have measured the wavelengths of magnetic dipole transitions between fine-structure levels in the ground term of Ti-like ions. Our theoretical results agree well with the experimental ones. The differences are less than 0.6% for elements below $Z=60$ and about 0.1% (0.4 nm) for those over $Z=60$ (the worst being 0.16% for $Z=83$). Although the accuracy in the range of $Z=51-56$ was worse than that over $Z=60$, the differences are not more than 0.6%. We can conclude that the present calculation may well predict unmeasured wavelengths of the same transitions along the Ti-like sequence, especially for higher Z elements. The list of wavelengths for elements other than those reported here will be presented in another paper [22]. The anomalous behavior predicted by Feldman, Indelicato, and Sugar [7] was confirmed by the experiments over a wide range of atomic numbers.

ACKNOWLEDGMENTS

This work was performed under the auspices of the International Cooperative Research Project (ICORP) of the Japan Science and Technology Corporation, and partly supported by a Grant-in-Aid for Scientific Research (B-1048099) from the Ministry of Education, Science, Sports and Culture of Japan.

[1] R. C. Isler *et al.*, Phys. Plasmas **4**, 355 (1997).
[2] K. Ida and S. Hidekuma, Rev. Sci. Instrum. **60**, 867 (1989).
[3] S. Suckewer and E. Hinnov, Phys. Rev. Lett. **41**, 756 (1978).
[4] D. Wróblewski *et al.*, Phys. Rev. Lett. **61**, 1724 (1988).
[5] E. Hinnov *et al.*, Phys. Rev. A **25**, 2293 (1982).
[6] K. H. Burrell *et al.*, Phys. Rev. A **29**, 1343 (1984).
[7] U. Feldman, P. Indelicato, and J. Sugar, J. Opt. Soc. Am. B **8**, 3 (1991).
[8] C. A. Morgan *et al.*, Phys. Rev. Lett. **74**, 1716 (1995).
[9] F. G. Serpa *et al.*, Phys. Rev. A **53**, 2220 (1996).
[10] J. V. Porto, I. Kink, and J. D. Gillaspy, Phys. Rev. A **61**, 054501 (2000).
[11] D. J. Bieber *et al.*, Phys. Scr. **T73**, 64 (1997).
[12] J. R. Crespo López-Urrutia *et al.*, Phys. Scr. **T80**, 448 (1999).
[13] S. B. Utter, P. Beiersdorfer, and G. V. Brown, Phys. Rev. A **61**, 030503(R) (2000).
[14] E. Träbert *et al.*, Phys. Scr. **58**, 599 (1998).
[15] D. R. Beck, Phys. Rev. A **56**, 2428 (1997).
[16] D. R. Beck, Phys. Rev. A **60**, 3304 (1999).
[17] F. J. Currell *et al.*, J. Phys. Soc. Jpn. **65**, 3186 (1996).
[18] H. Watanabe *et al.*, J. Phys. Soc. Jpn. **66**, 3795 (1997).
[19] V. Kaufman and J. Sugar, J. Phys. Chem. Ref. Data **15**, 321 (1986).
[20] T. A. Carlson *et al.*, At. Data **2**, 63 (1970).
[21] F. A. Parpia, C. F. Fischer, and I. P. Grant, Comput. Phys. Commun. **94**, 249 (1996).
[22] D. Kato *et al.* (unpublished).
[23] J. R. Crespo López-Urrutia *et al.*, Lawrence Livermore National Laboratory, EBIT Annual Report 1995, 26 (1996).